Alignment Control of an Optical Link in a Turbulent Channel for Satellite Communication Systems

Ana Carolina Teixeira Borralho
ana.borralho@tecnico.ulisboa.pt

Instituto Superior Técnico, Lisboa, Portugal

November 2021

Abstract

The use of satellites in communications has revolutionized the transmission of information, allowing to interconnect increasingly distant points. Radio frequency systems have been used for a long time. However, they are facing spectrum congestion and difficulty in meeting the current requirements of bit rate, bandwidth, security and capacity. Optical systems began to be explored and their multiple advantages over radio systems have made them an interesting alternative for Earth-space communications.

Optical systems achieve high accuracy by using narrow laser beams, which makes the alignment between terminals extremely challenging when a satellite is in orbit. In addition, the effects of the propagation in the atmosphere result in further degradation of the signal caused. These problems are magnified when we refer to small satellites, due to their size, weight and power constraints.

The objective of this dissertation is to study a closed loop pointing system that optimizes the alignment between terminals of an optical communication between a small satellite in low orbit and the Earth, test the system under atmospheric turbulence conditions and perspective the feasibility of a long range link.

The implemented pointing system receives the uplink beacon and corrects the position of the downlink signal so that there is alignment. The position control was done using a closed loop proportional, integral and derivative control system that allows corrections until 3.4 mrad. The system was set up experimentally and tested under turbulent conditions, showing that is possible to improve the link performance.
Keywords: Optical communications, Satellite communications, Free space optics, Pointing, acquisition and tracking, Closed loop alignment control, Atmospheric turbulence.

1. Introduction

Communication is one of the most important activities of the humanity. The desire to communicate remotely propelled the appearance of long haul communication systems. These started with wired connections, firstly with electrical cables and later with optical fiber. But the demand to connect increasingly distant points ended up showing that there are some situations where it is impossible or impractical to use wires [1]. This led to the interest in wireless communications, and as communication technologies evolved, satellites appeared and became a promising technology for long haul communication and to connect points where terrestrial systems cannot access [2].

The satellite communication started being explored using the radio frequency (RF) domain, but these systems find it difficult to meet all the requirements posed nowadays. The demand for high bit rate, bandwidth and capacity has grown significantly in recent years, leading to the congestion of RF spectrum and the search for alternatives. The growing studies in the field of optics revealed optical communications systems as a very interesting option [3].

Optical wireless communication (OWC) systems offer many advantages over RF systems such as large available bandwidth, high data rate, license free spectrum, less power consumption and low mass requirements and high security, so it is easy to see their potential for high-speed broadband connections [4]. Outdoor OWC, better known as free space optics (FSO), allow information to be transmitted using an unguided channel, which is the case of atmospheric propagation. Furthermore, FSO makes it possible to establish ground-to-satellite, satellite-to-ground and satellite-to-satellite links.

However, the performance of optical links is affected by many factors such as beam divergence over long distances, pointing errors, strong atmospheric attenuation and atmospheric turbulence [1]. These factors cause degradation and in extreme cases, even loss of the link. Therefore,

emerges the necessity of developing pointing systems that optimize the alignment between emitter and receiver terminals, maintaining their line of sight and further enhance optical communication. The pointing requirements of a satellite are generally "beyond the satellite's body pointing capability" [5], specially in small satellites due to their size, weight and power constraints, requiring fine pointing stystems that attain higher accuracies.

1.1. State of the Art

The advances in the field of space technology unlocked the door for optical communications in space and emerged the idea of creating an all optical communication architecture to respond to the increasing demand for large capacity and high data rate. FSO technology has developed to the point that today it is possible to transmit high rates of several gigabits per second over many kilometers [1]. Many experiments have been done to demonstrate the feasibility of optical links, including ground-to-satellite, satellite-to-ground and satellite-to-satellite [4]. The technology that allowed to attain higher data rates was the wavelength division multiplexing (WDM) and it was first demonstrated in 1999, by using four optical channels, carrying a 2.5 Gbps signal each, over a distance of 4.4 km [6]. Meanwhile, FSO experiments with mobile terminals started being conducted and it was demonstrated a full-duplex communication link between two balloons at 20 km of altitude, attaining a 130 Mbps bit rate and exceeding distances of 100 km [7]. It was also reported the transmission between ground terminal and a moving unmanned arial vehicle (UAV) separated by 50 m, with a 80 Gbps bit rate [8].

It is relevant to mention that in more recent years an interest in quantum key distribution (QKD) applications propelled the development of quantum FSO communications. In particular, the satellite-to-Earth quantum FSO has been a popular subject of study with significant progress [9]. It was demonstrated a free-space satellite-to-ground QKD transmission between Micius satellite and Xinglong ground station, at a distance of 1200 km. However, the deployment of quantum FSO systems still needs to overcome multiple issues, for example the perturbation that turbulence causes to quantum states.

Further techniques have been developed to improve the performance of FSO systems [4], such as channel coding, diversity, adaptive optics, hybrid RF/FSO systems and relay-assisted transmission.

1.2. Objectives

The main objective of this dissertation is to study a closed loop pointing system that optimizes the alignment between emitter and receiver of an optical downlink communication, minimizing the effects of turbulence. In order to achieve the overall objective it is necessary to attain sectorial subobjectives, namely: (1) Implement a close-loop control system to maximize the alignment of the optical beam, (2) Test the pointing algorithms under atmospheric turbulence effects and (3) Perspective the feasibility of a long range optical link.

2. Optical Communications Background

This chapter gives some background about optical communications system, namely the description of a typical FSO communication system and factors that affect its performance such as modulation schemes, channel noise and atmospheric propagation. Section 2.3 describes a pointing, acquisition and tracking sequence and system.

2.1. Optical communications

A typical FSO communication system is depicted in Fig. 1. The transmitter could be a laser diode or a high-intensity LED. It produces a modulated beam and transmits it towards the receiver. As it propagates, the beam suffers some losses due to channel effects.

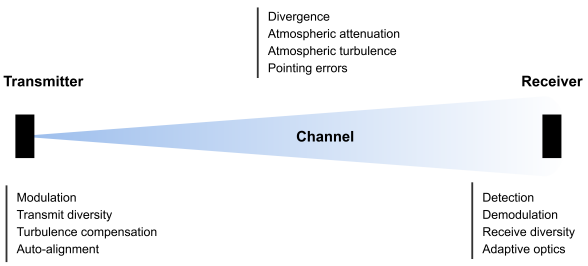

Figure 1: Typical FSO communication system, adapted from [1].

To evaluate the performance of the link it can be useful to use the metric signal-to-noise ratio, SNR. According to [10], it can be written as expression 1, where $R(\lambda)$ is the photodetector's responsivity at the operating wavelength, P_r is the received optical power and the parameters σ_{shot} and σ_{thermal} are the shot noise and thermal noise variances, respectively.

$$\text{SNR} = \frac{S}{N} = \frac{(R(\lambda)P_r)^2}{\sigma^2_{\text{shot}} + \sigma^2_{\text{thermal}}} \tag{1}$$

The received power depends on the modulation/demodulation scheme used and on the main channel effects such as beam divergence, attenuation, turbulence and pointing errors.

2.1.1 Modulation and demodulation

The intensity of an optical source varies according to the amplitude of a modulating signal, so the

most simple and common method for FSO applications is intensity modulation. However, phase modulation is used with optical signals if very high data rates are required. The detection system can be incoherent (more known as direct) or coherent, but usually intensity modulation is associated with direct detection.

Some IM/DD schemes are pulse amplitude modulation (PAM), on–off keying non-return-to-zero (OOK-NRZ) is a subset of PAM, pulse position modulation (PPM), digital pulse interval modulation (DPIM) and sub-carrier intensity modulation (SIM). This last one allows modulation formats that also make use of phase [1]. The information can also be encoded using real-valued orthogonal frequency division multiplexing (OFDM) signals. There are two major OFDM techniques: asymmetrically clipped optical (ACO) OFDM and DC biased optical (DCO) OFDM [11]. These are all suitable for small satellites, since they offer bandwidth and power efficiency, low implementation complexity and robustness to ISI.

2.1.2 Channel noise

In FSO systems, noise is mainly introduced at the receiver. Its bandwidth, Δf, is related with the noise power so that the wider the bandwidth of the detection system, the more noise results. The main sources of noise are thermal noise, derives from the thermal fluctuations of the electrons in the receiver circuit conducting material, and shot noise, provoked by the movement of electrons in the photodetector.

The total output noise power is given by [1]:

$$N = P_n G + P_a = ((\sigma_{\text{th}}^2 + \sigma_{\text{shot}}^2)\sqrt{\Delta f})G + P_a \quad (2)$$

It depends of the input noise power P_n, of the gain of the amplifier G and of the noise contribution of the amplifier P_a. Finally this parameter, N, can be used to calculate the SNR and thus evaluate the performance of the receiver.

2.2. Propagation in the atmosphere

The propagation of a light beam in the atmosphere includes some challenges that may complicate and impair its reception.

Beam divergence

A laser beam leaves the emitter with a certain diameter, and it widens with a divergence angle θ_{div} as it propagates. When it reaches the receiver at a distance L, the diameter is much wider, and thus part of the signal is dissipated and only part hits the detector, resulting in substantial decrease of the received power.

Atmospheric attenuation

The propagation of a laser beam through the atmosphere includes absorption and scattering by particles in the medium, depending on their size and concentration.

When choosing the wavelength of a FSO system it should be taken into account the atmospheric absorption spectrum. Normally the choice goes to a wavelength that corresponds to minimal absorption and the absorption can be ignored in comparison to the scattering effects.

Atmospheric turbulence

The atmospheric turbulence results from air temperature fluctuations that vary randomly in space. The random regions are called cells and when a laser beam propagates through them it suffers aberrations that lead to wavefront distortions and intensity fluctuations. The effects observed in the received power are scintillation and beam wander.

Pointing errors

The alignment between terminals is challenging since a satellite terminal is in movement and its link must operate over long distances. Inherently, when the signals are transmitted there will be pointing errors and if the misalignment between terminals becomes too big it can result in partial or total loss of the signal [1].

2.3. Pointing, Acquisition and Tracking

The alignment between emitter and receiver is essential for the success of an optical communication. A pointing, acquisition and tracking (PAT) system is responsible for searching a laser beam coming from the other terminal and orientate its own terminal in that direction, with the aim to establish a link while tracking the opposite terminal. Fig. 2 illustrates a PAT sequence:

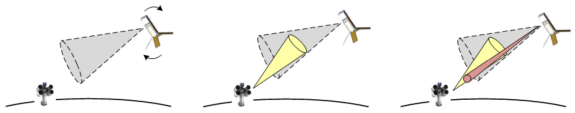

Figure 2: Pointing, acquisition and tracking sequence, adapted from [12].

(1) **Pointing:** In the first phase, coarse pointing is performed, giving a rough estimate of the ground station position. The satellite begins a slew maneuver to point in that direction with the aim that the GS will be visible within the beacon detector's field of view (in grey). (2) **Acquisition:** With both terminals roughly aligned, the ground station tracks the satellite and transmits an uplink beacon (in yellow) that will be acquired by the satellite and begin the fine pointing. (3) **Tracking:** Fine pointing starts and the beacon is now continuously tracked during the communication window, so the satellite can transmit the downlink signal (in red) towards the ground station.

PAT System

A typical PAT includes a coarse pointing system that uses a wide field of view detector and a fine pointing system with a narrow field of view that provides high precision. The key elements of a fine pointing system are a detector and a mobile element to control the alignment of uplink and downlink beams. The last one can be a MEMS FSM (micro electro mechanical system fast steering mirror) to adjust the downlink signal orientation, or some electromechanic device to control directly the position of the downlink signal.

The most used detectors are quadrant detectors/quadcells and cameras. A quadrant detector is equivalent to a camera of only four pixels. When a laser beam hits a quadrant detector, each quadrant generates a photocurrent, depending on the intensity. To estimate the position of the beam in both x and y axes, we can use expressions $X = \frac{(i_A+i_D)-(i_B+i_C)}{i_A+i_B+i_C+i_D}$ and $Y = \frac{(i_A+i_B)-(i_D+i_C)}{i_A+i_B+i_C+i_D}$ from [13]. Quadcells have shown to be advantageous as it requires much less processing and memory than a camera. However, cameras are more versatile since they are used in satellite missions that include imaging and they serve other beam diagnostic purposes. An image captured by a camera gives a full intensity profile, and thus the position of the beam can be determined through an image processing algorithm that computes the beam centroid.

3. Fine Pointing System

3.1. Pointing systems in nanosatellites

In this section we will present and describe some fine pointing systems used in nanosatellites in prior missions that served as a reference for this master thesis. In 2017, Massachusetts Institute of Technology Space, Telecommunications, Astronomy, and Radiation Laboratory (MIT STAR Lab) developed a precision closed loop laser pointing system for the Nanosatellite Optical Downlink Experiment (NODE) [5] that was able to attain a 20 μrad pointing accuracy. Its optical diagram is illustrated in Fig. 3.

NODE receives the uplink beacon from the optical ground station and detects it on a camera. Two internal laser sources are generated: the downlink signal and the calibration signal. This last one is the main character of the closed loop pointing system, since its sampling on the camera works as direct optical feedback of the FSM pointing angle. After a ray geometry analysis, the author of [5] identified that the side mirror causes backwards reflection of the calibration beam (in red), explaining that uplink and downlink signals must have opposite angles of incidence at the lens to have optimal alignment. This implies that the calibration laser has to have a symmetric relation with the uplink

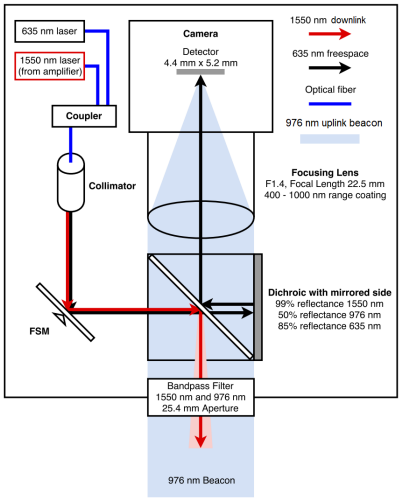

Figure 3: Optical diagram of NODE, from [5].

beacon in relation to a center of symmetry, which corresponds to the center of the camera.

More recently, in 2020 it was developed a high accuracy pointing method (Fig. 4) that was tested in a satellite-to-ground quantum communication with the quantum science satellite Micius, with demonstrations of 0.5 to 1 μrad pointing accuracy [14].

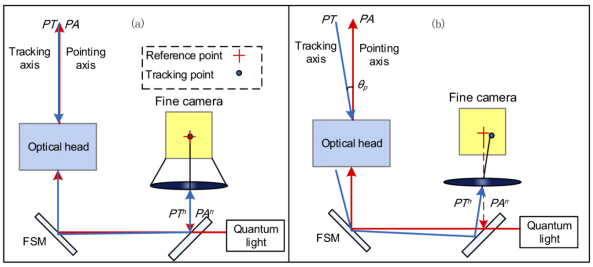

Figure 4: Principles of the fine pointing system used on Micius, from [14].

This fine pointing system uses a quadrant detector and it does not use an internal calibration laser. As we can see in Fig. 4, the two signals involved are: the ground station beacon (blue line) and the downlink quantum signal (red line). When the GS beacon reaches the fine pointing system on the satellite, it is reflected in a fast steering mirror, then in a simple mirror and finally detected by the quadcell. The alignment of red and blue lasers is guaranteed when the FSM is adjusted so that the blue line is on the reference point of the quadcell (Fig. 4). This way, the downlink signal leaves the satellite with the same direction as the uplink.

3.2. Pointing system proposal

After analysing the two pointing systems presented in section 3.1, and taking into account the required simplicity, the design we came up with is illustrated in a diagram in Fig. 5. The design is very similar to NODE (Fig. 3) but there are two major differences:

(1) Only one signal is generated in the satellite and it is a red laser used for calibration and at the same time it is modulated and transmit data to the ground station receiver, (2) We do not use a FSM to control the alignment between uplink beacon and calibration beam, instead we assemble our laser on a kinematic mount that allows to control directly the position of the laser.

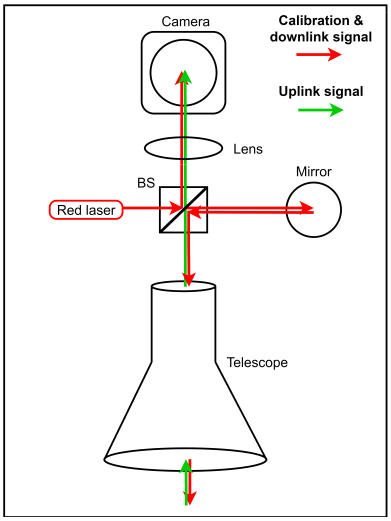

Figure 5: Optical diagram.

Looking at Fig. 5, the uplink beacon (in green) comes from the ground station and it is detected on the camera. The calibration laser (in red) is also detected on the camera so we can compute the distance between green and red spots and adjust the position of the calibration laser in order for the spots to be overlapped. At the same time, the red signal (modulated) is transmitted as downlink signal, and when the pointing control works, it leaves the satellite with the same orientation as the uplink beacon, going toward the ground station, where it is detected.

3.3. Closed Loop Control

The pointing objective is to follow a dynamic reference, in this case, the uplink beacon disturbed by atmospheric turbulence. The diagram in Fig. 8 represents the closed loop control pointing system. The fine pointing begins when the camera acquires an image containing green and red laser beams. Their centroids in the image (in pixels) are calculated by an image processing algorithm. The difference between centroids is the pointing error and the correction intends to bring the centroids closer.

We chose to use a proportional, integral and derivative (PID) controller. The error feeds the closed loop and the correction applied is given by equation 3 [15], where $p(t)$ is the new position and p_0 is the current position of the calibration laser, K_p, K_i and K_d are the proportional, integral and

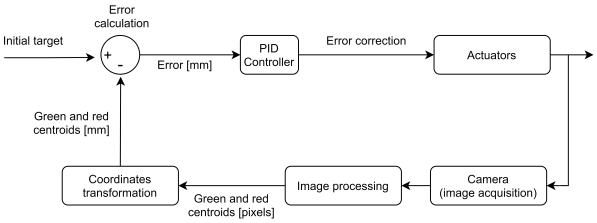

Figure 6: Closed loop control system.

derivative gains and $e(t)$ is the error.

$$p(t) = p_0 + K_p e(t) + K_i \int_0^t e(\tau)\mathrm{d}\tau + K_d \frac{\mathrm{d}e(t)}{\mathrm{d}t}, \quad (3)$$

An optimal combination of proportional, integral and derivative gains allows a faster and more stable system response.

Active Control

The fine pointing begins when the camera takes one frame (Fig. 7). An image processing algorithm developed in Matlab is applied to identify the beams separately and calculate their centroids. It is useful to determine a correlation between the kinematic mount *x* and *y* position of the red laser and its projection on the camera (its centroid), so we know what correction we have to apply to the kinematic mount for the red centroid follows the green. Knowing that the correlation is linear, we proceed to calculate the error illustrated in Fig. 7.

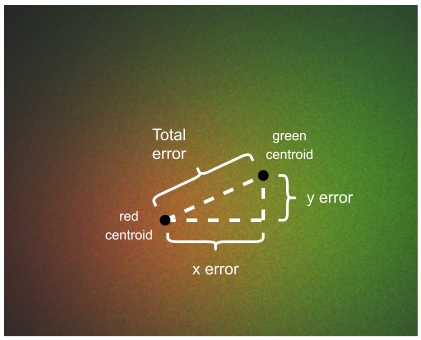

Figure 7: Illustration of the alignment error. It corresponds to the distance between red and green spots in x and y axes.

It translates the distance between centroids:

$$\text{error} = \text{target centroid} - \text{calibration centroid}. \quad (4)$$

The final step of the fine pointing loop is to apply a correction to the calibration laser position with the aim to align it with the target, or at least bring them closer. The correction can be just adding the error to the red laser current position, nevertheless, when using PID control, the expression of the new position has to include the proportional, integral and derivative terms in 3. The choice of the gain values, integral and derivative of the error will be done experimentally in section 4.2.

3.4. Modelling and simulation

In order to better understand the control loop it was essential to do some simulation work. This allows to model the dynamic elements of the control chain such as the camera, the controller and the kinematic mount responsible for moving the calibration laser, and see their influence in the loop. The closed loop control system was created using the Matlab Simulink environment and it is represented in Fig. 8.

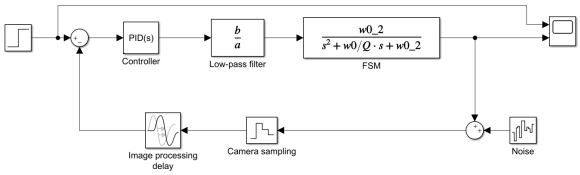

Figure 8: Closed loop system created in Matlab Simulink.

Since we could not determine a transfer function for our kinematic mount, we considered the usage of the FSM used in the NODE simulation scheme [5]. The first dynamic element of the loop is the camera. It works at a certain sampling rate, however, the FSM's dynamics are much slower, making them the most limiting element of the system and thus the focus of the model. Nevertheless, image acquisition and processing can influence significantly the loop, due to noise that gets to the camera and to the time delay caused by the centroid computation.

Moving to the FSM, its model is simple, since their manufacturer gave an exclusive datasheet, where the FSM specifications needed to determine its transfer function are discriminated, such as resonant frequency w_0 and quality factor Q. The dynamic model is given by second order transfer function, where the input is a driving voltage and the output is the new angular position of the FSM:

$$\frac{\theta_{FSM}(s)}{V_{driving}(s)} = \frac{w_0^2}{s^2 + \frac{w_0}{Q}s + w_0^2}, \tag{5}$$

The FSM step response was extremely ressonant, so to fix this it was placed an analog low-pass filter at the FSM entrance. In the LPF block in Fig. 8, "b" and "a" are transfer function coefficients.

At last, we used the Simulink Control Design Toolbox to tune the PID controller. The definition of the PID gains have significant impact in the way the system responds and adapts. They make the response faster or slower, more robust or more aggressive. For this particular case, the automatic tuning suggested the best gain parameters to be K_P=0.1471, K_I=0.5111 and K_D=-0.2236.

4. Experimental Implementation

4.1. Experimental setup

An experimental testbed is essential to test and validate the control algorithms in a more real situation. The setup is represented in a diagram in Fig. 9. On the right side we have the block representing the optical ground station, which we consider to be the emitter, and on the left side is the satellite receiver. The uplink beacon (in green) is transmitted from the ground station to the satellite, entering the telescope and being detected on the camera. Then the control algorithms are performed for alignment. Once this happens, the red modulated laser is reflected in a simple mirror and leaves the satellite with the same orientation as the green laser, being received at the ground station's detector.

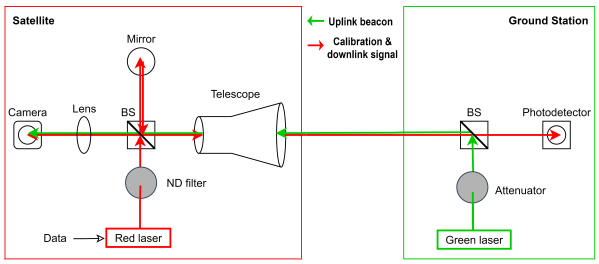

Figure 9: Diagram of the setup assembled in the laboratory.

The real setup assembled on the laboratory is shown in Fig. 10. It is important to mention that all optical components were manually mounted and aligned on the optical board, which can lead to major alignment errors.

The optical ground station corresponds to Fig. 10 (b) and it comprises the uplink beacon, a beam splitter from Thorlabs with a 50:50 beamsplitting ratio, an attenuator that is a 1.0 optical density absorptive ND filter to reduce the laser intensity when it hits the camera on the satellite, and a detector. The detector used was the Thorlabs DET10A2, which is a biased silicon detector with an active area of 0.8 mm^2 and a wavelength range from 200 to 1100 nm. It is positioned on the ground station to receive the downlink signal.

Fig. 10 (a) shows the assembly of satellite fine pointing system. On the bottom we see the telescope and another Thorlabs 50:50 beam splitter. On the left we have the downlink and calibration laser assembled on its kinematic mount that is operated by two controllers and stages (one for each axis). Between the laser and the beam splitter there is a 1.3 optical density absorptive ND filter, responsible for attenuating the intensity of the red laser so it does not saturate the camera. On the right we see the simple mirror responsible for reflecting the red laser for it to follow its path towards the ground station. Finally, on top, we have the tracking camera and added a convex lens from Thorlabs with a focal distance of 3 cm, with the pur-

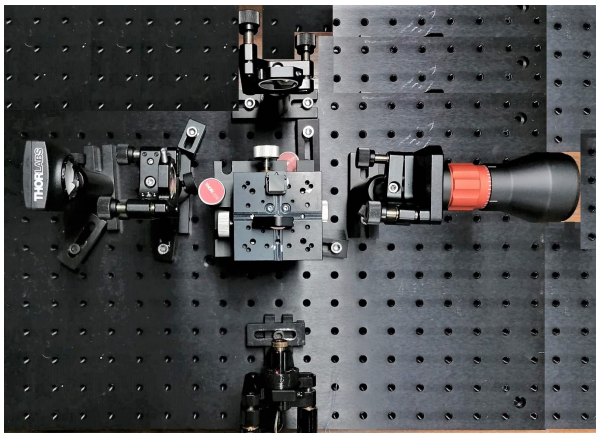

(a) Satellite's fine pointing system.

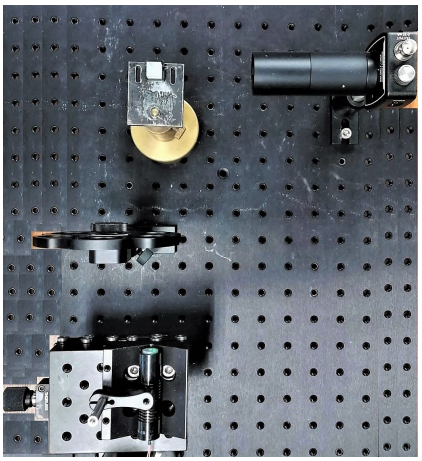

(b) Optical ground station.

Figure 10: Experimental setup.

pose of reducing and focus the beams. Otherwise, their spots would be very large when they reach the camera.

Required Equipment

For the **uplink beacon** from the optical ground station it was considered a Roithner green laser working on 520 nm with a power of 5 mW. This power is too high to be detected on the camera, causing full saturation of the image, and thus the 1.0 optical density absorptive ND filter and the convex lens are used, to reduce the intensity and the size of the beam, respectively. The uplink beacon is very large when arrives to the satellite, so the objective of the **telescope** is to reduce its size, keeping the collimation. The Thorlabs Fixed Magnification Beam Expander GBE05-B has 5X beam reduction

The **downlink and calibration laser** is a 40 mW 650 nm laser from Roithner. It supports TTL modulation, so we used an arduino to modulate it by just switching it on and off, and thus transmit data as a downlink signal. At the same time, its main function is the internal calibration. The laser is detected on the camera and it follows the green laser, aiming to keep receiver and emitter aligned. This laser is assembled on a Thorlabs Precision **Kinematic Mirror Mount** KS2 in order to control its position. This mount holds 50.0 mm optics and has 3 adjusters, allowing angular adjustment of ±4 °in x and y axes. These axes are controlled by two Thorlabs Kinesis® KDC101 K-Cube™ Brushed DC Servo Motor **Controllers**. They allow manual and/or automatic control of DC Servo motors using their own motion control software Kinesis or in this case, using Matlab. The compatible **stages** are the Thorlabs Z812. They actuate on the kinematic mount and have a total range of 12 mm in each axes and a maximum velocity of 2.6 mm/s.

The chosen model for the **camera** was the Thorlabs DCC1645C USB 2.0 CMOS Camera. Some of its characteristics are a color sensor type, effective number of pixels of 1280 x 1024 and imaging area of 4.61 mm x 3.69 mm and a maximum frame rate of 24.9 fps. The imaging area is very small, which is why it was so important to insert the convex lens before the camera. To avoid saturation of the acquired images, it was placed a piece of tracing paper right in front of the detector. This method allowed to cut some of the intensity of the beams without using another attenuator.

4.2. Experimental implementation

The first step was to connect and conFig. the hardware (camera, controllers and stages) using Matlab. We started by testing the range of positions of the red laser that are detected within the camera's field of view and concluded that the beam is present in the image when the controller position is between $x \in [0.6, 3.2]$ millimeters and $y \in [0.2, 2.1]$ millimeters. It was determined a linear correspondence between the kinematic mount x and y position [mm] and the projection of the red laser on the camera [pixels]. Then we started the tests to the image processing algorithm that detects and calculates the beam centroids. The green laser was static, so we simulated a turbulent environment using 3 lamps of 100 W each connected to power supply. The green laser passes right above the lamps and their overheating provokes disturbance of the beam, just like the uplink beacon is disturbed when it passes the atmosphere towards the satellite.

Passing to the test of the control algorithms, when the control loop starts, the camera acquires an image similar to Fig. 7, with a red and a green spots. It goes through image processing and the centroids are estimated. The green centroid is set as the reference and the error is computed in both x and y axes. It is convenient to present the pointing error in radians, and considering the distance L

from the emitter to the telescope and Δx the range of positions of the emitt ing laser that are detected on the camera, it was concluded that the proposed system allows corrections until of 2α = 3.4 mrad. Assuming a LEO-to-ground communication where L=500 km, the pointing range Δx at the Earth surface is in the order of 0.5 km, which is much higher than the receiver telescope.

The last step of the control loop is to calculate the correction and actuate, changing the position of the calibration laser to follow the reference. The correction calculation depends on the type of control. When using proportional control, it is considered K_p=1 and K_i=K_d=0, meaning that the correction is the sum of the laser current position with the error value. When using PID control it used the expression 3 to estimate the correction. To calculate the integral and the derivative terms of the expression, it was considered the plot of the *x* error over time obtained with proportional control (plot available in section 4.3). The values considered for *x* axis were $\int_0^t e_x \mathrm{d}\tau$ = 0.1190, $\frac{\mathrm{d}e_x(t)}{\mathrm{d}t}$ = 0.0027, and for *y* axis $\int_0^t e_y \mathrm{d}\tau$ = 0.0089 and $\frac{\mathrm{d}e_y(t)}{\mathrm{d}t}$ = 0.0198. With these values fixed, we varied the gain values K_p, K_i and K_d between 0.1, 1 and 10 to see their clear influence in system response.

4.3. Experimental Results

4.3.1 Control Tests

In this section we will present the results of the tests performed, always running the control system for 100 cycles. We thought it was interesting to start testing a system that does not use control (it receives the uplink beacon from the ground station but it does not move in response to it) and compare it with proportional control with K_p=1 (meaning the correction to apply is equal to the error). In Fig. 11 we can see the error scatters.

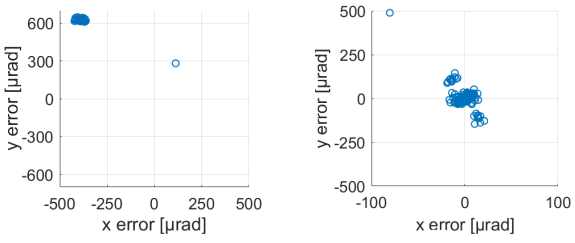

Figure 11: Error scatter when the FPS (a) does not use any control (b) uses proportional control with $K_p = 1$.

We can see that without control (Fig. 11 (a)) the error is always very far away from zero and the total pointing error has a mean of 697 µrad. Using proportional control (Fig. 11 (b)), the error oscillates around zero and the total pointing error mean is 42.5 µrad, which is more than 10 times less than no control.

We will now summarize the results of the study of the variation of the gains of a **PID control** system. We gave the gains the values 0.1, 1 and 10 and examined the difference it makes to the system response.

To study the effects of the proportional gain K_p, we fixed K_i=K_d=0.1. When K_p=0.1 the system is slow to respond and has a mean total error of 112.5 µrad. The low K_p not have enough strength to correct the error completely, creating an error offset. With K_p=1 we get the fastest response, with the error in each axis oscillating around zero, and a lowest mean total error of 45.7 µrad. It is the most adequate to follow the reference quickly and to guarantee the alignment. For the highest K_p value, we tried 10, 5 and 2, but all caused a poor system response: very slow and with a significantly higher mean total error. The slowness is because the correction to apply is so big that the calibration laser moves much more to correct the error.

To study the impact of the integral gain, we fixed K_p=1 and K_d=0.1. The increase of K_i has some pros such as making the laser movement more subtle and thus the time to complete 100 cycles is less. However, it has also showed cons such as the increase of the mean average error from 45.7 µrad to 797.4 µrad and the appearance of an offset in the *x* and *y* errors, indicating there is always an error between the two lasers and thus they are never truly aligned. The integral gain that led to better results was then K_i=0.1.

Finally, we fixed the parameters that led to better results before K_p=1 and K_i=0.1, and varied K_d. The mean total error is 45.7 µrad for K_d=0.1, 34.1 µrad for K_d=1 and 140.3 µrad for K_d=10. The increase of the gain, made the movement of the laser and the error over time smoother, but the same similarly to K_i the, the error in each axis gets a slight offset. The fact that the derivative terms $\frac{\mathrm{d}e_x(t)}{\mathrm{d}t}$ = 0.0027 and $\frac{\mathrm{d}e_y(t)}{\mathrm{d}t}$ = 0.0198 are so small, makes them to have the least effect in the system response. Even when we raise K_d to 10, the mean total error increases but not as abruptly as when we raise K_p or K_i. Also, it does not influence significantly the time it takes to complete the 100 cycles.

Optimized condition

Analyzing the previous section, the gain combinations that present the lowest mean total errors are K_p=1, K_i=0.1 and K_d=0.1 and (b) K_p=1, K_i=0.1 and K_d=1. Their scatter errors are presented in Fig. 12.

It is notorious that 12 (b) shows less dispersion, making it a better option, but that does not imply that (a) is not valid. The truth is that both op-

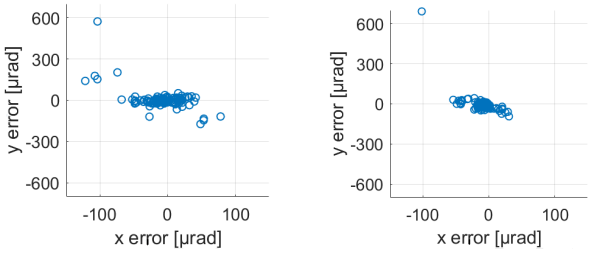

Figure 12: Scatter error for (a) K_p=1, K_i=0.1 and K_d=0.1, (b) K_p=1, K_i=0.1 and K_d=1.

tions can be considered adequate, depending on the accuracy requirements of the satellite mission. If the error is less than the accuracy requirement, it means the downlink signal will be received properly. In this case, the error offset present in (b) means the signals are not totally aligned but that does not impede a correct downlink reception.

4.3.2 Downlink data reception

The last objective of the this thesis is to demonstrate the downlink feasibility for communication. The red laser is modulated and makes its way to the ground station (downlink), passing the turbulent channel created with the lamps, to simulate the atmosphere. The ground station detector is connected to an oscilloscope so the received signal is observed in Fig. 13.

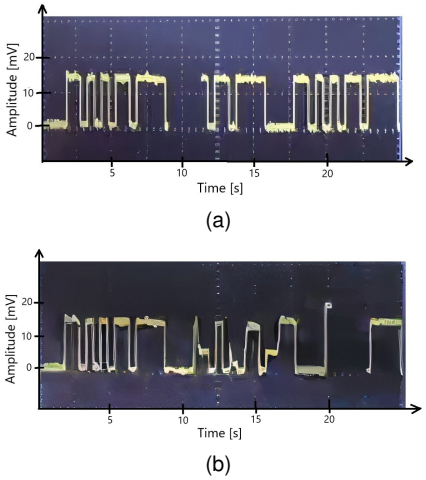

Figure 13: Downlink signal received in the ground station detector, observed in a oscilloscope.
(a) Closed loop pointing, (b) Without pointing control.

In the first situation, it was used the PID control with gains K_p = 1, K_i = 0.1 e K_d = 0.1. The received downlink signal can be seen in a normal mode in Fig. 13 (a). We observe the two levels of the signal that correspond to levels 1 and 0 of the binary message, leading to the conclusion that there is good reception of the signal.

In the second situation, Fig. 13 (b), it was tested the transmission of the downlink signal when the fine pointing system does not use any pointing control (approach used in Fig. 11 (a)). The signal path is the same as in the previous experience, but in this case, when the downlink signal passes the turbulent channel and the beam is disturbed, the system does not respond, compromising the signal reception. The received signal can be seen in a normal mode in Fig. 13 (b). It is noticeable that there are three power levels, instead of two, which does not correspond to the binary message. This happens because when there is a partial misalignment between terminals, only part of the power is received, creating a third level in between 1 and 0. This proves that is essential to use pointing control to guarantee a correct downlink reception.

5. Conclusions

Given the fact that optical communications are being highly explored for satellite systems, this thesis proposed to implement a closed loop pointing solution that promotes the alignment between an optical ground station and a moving terminal of a satellite.

It was given an overview of optical communications, namely of a pointing, acquisition and tracking sequence and system. It was made a proposal for the pointing system to study, where the system receives the uplink beacon coming from the ground station and uses a calibration laser assembled on a kinematic mount to track it using a closed loop PID control. An image processing algorithm was developed to detect both uplink and calibration spots on the tracking camera and calculate their centroids, and also a control algorithm responsible for tracking the uplink beacon with the calibration beam. Some computational simulation of the closed loop control system was done, concluding that the dynamic elements of the active control have significant impact on the system response and performing control tuning.

Experimentally, it was assembled the proposed pointing system and a block that represents the optical ground station. The uplink beacon was done with a 520 nm laser and the downlink with a 650 nm laser and it was obtained an optimal pointing condition using the PID gain parameters: K_p=K_d=1 and K_i=0.1. Given the assemble, it was concluded that the system can correct errors of a maximum of 3.4 mrad of divergence. For a LEO-to-ground communication at a distance from the Earth of 500 km, this pointing range corresponds to approximately 500 m, which is much greater than the receiver telescope. This value assures a perspective of feasibility for a long range communication. Finally, the downlink data reception was observed when the

optimized pointing control system was used and confirmed a good reception, seeing the transmitted binary message. Assuming the inherency of the optical communication system, namely the low attenuation of the channel conjugated with the tracking solution here proposed, we consider this as a feasible solution for a long range connection.

5.1. Future Work

For this work to fulfil its objective of controlling the alignment, there are two corrections to apply to the pointing system: (1) Develop an algorithm that applies a correction to the calibration laser that instead of overlapping the two beams, sends the calibration laser to the symmetric position of target, being the center of symmetry the center of the camera. Using a side mirror on the optical design, this is a way to achieve accurate pointing. (2) Optimize the integral and derivative terms of the PID controller to try to obtain a better PID response or even explore new types of controllers that might be adequate for this application.

After these improvements are made, future work might be to implement all the control chain algorithms in a microcontroller and test them integrated in a satellite payload. This fine pointing system can be associated to a coarse pointing system to improve the global pointing accuracy and be integrated in a small satellite.

References

[1] A. Trichili, M. A. Cox, B. S. Ooi, and M.-S. Alouini, "Roadmap to free space optics," *Journal of the Optical Society of America B*, vol. 37, no. 11, pp. 184–201, 2020.

[2] H. Willebrand and B. Ghuman, "Fiber optics without fiber," *IEEE Spectrum*, vol. 38, pp. 40–45, Sept 2001.

[3] V. Chan, "Optical space communications," *IEEE Journal of Selected Topics in Quantum Electronics*, vol. 6, pp. 959 – 975, Dec 2000.

[4] H. Kaushal and G. Kaddoum, "Optical communication in space: Challenges and mitigation techniques," *IEEE Communications Surveys Tutorials*, vol. 19, no. 1, pp. 57–96, 2017.

[5] O. Cierny, "Precision closed-loop laser pointing system for the nanosatellite optical downlink experiment," Master's thesis, Luleå University of Technology, 2017.

[6] G. Nykolak, P. F. Szajowski, J. Jacques, H. M. Presby, J. A. Abate, G. E. Tourgee, and J. Auborn, "4×2.5 Gb/s 4.4 km WDM Free-Space Optical Link at 1550 nm," in *Optical Fiber Communication Conference and the International Conference on Integrated Optics and Optical Fiber Communication*, vol. Supplement. Optical Society of America, 1999, pp. PD11/1–PD11/3 Suppl.

[7] B. E. Moision, B. I. Erkmen, E. Keyes, T. Belt, O. Bowen, D. Brinkley, P. L. Csonka, M. L. Eglington, A. Kazmierski, N. Kim, J. Moody, T. Tu, and W. Vermeer, "Demonstration of free-space optical communication for long-range data links between balloons on Project Loon," in *LASE*, 2017.

[8] L. Li, R. Zhang, Z. Zhao, G. Xie, P. Liao, K. Pang, H. Song, C. Liu, Y. Ren, G. Labroille, P. Jian, D. Starodubov, B. Lynn, R. Bock, M. Tur, and A. E. Willner, "High-Capacity Free-Space Optical Communications Between a Ground Transmitter and a Ground Receiver via a UAV Using Multiplexing of Multiple Orbital-Angular-Momentum Beams," *Scientific reports*, vol. 7, no. 1, p. 17427, Dec 2017.

[9] S.-K. Liao, W.-Q. Cai, and W.-Y. Liu, "Satellite-to-ground quantum key distribution," *Nature*, vol. 549, no. 7670, p. 43–47, 2017.

[10] D. R. Kolev and M. Toyoshima, "Received-Power Fluctuation Analysis for LEO Satellite-to-Ground Laser Links," *Journal of Lightwave Technology*, vol. 35, no. 1, pp. 103–112, 2017.

[11] R. Mesleh, H. Elgala, and H. Haas, "On the Performance of Different OFDM Based Optical Wireless Communication Systems," *Journal of Optical Communications and Networking*, vol. 3, no. 8, pp. 620–628, 2011.

[12] R. Kingsbury, K. Riesing, and K. Cahoy, "Design of a free-space optical communication module for small satellites," https://digitalcommons.usu.edu/smallsat/2014/AdvTechComm/6/, 2014, [Accessed: October 2021].

[13] Q. Li, H. Guo, S. Xu, Y. Xu, Q. Wang, D. He, Z. Peng, and Y. Huang, "TRC-Based High-Precision Spot Position Detection in Inter-Satellite Laser Communication," *Sensors*, vol. 20, p. 5649, Oct 2020.

[14] L. Zhang, J. Dai, C. Li, J. Wu, J. Jia, and J. Wang, "Design and in-orbit test of a high accuracy pointing method in satellite-to-ground quantum communication," *Opt. Express*, vol. 28, no. 6, pp. 8291–8307, Mar 2020.

[15] Wikipedia, "PID controller - Wikipedia, the free encyclopedia," http://en.wikipedia.org/w/index.php?title=PID\%20controller&oldid=1052917271, 2021, [Accessed: September 2021].